CASE STUDY OF A REINFORCED SOIL SLOPE WITH MARGINAL BACKFILL AS A DETENTION POND IN FLOOD CONTROL

Nelson N.S. Chou [1], Kuo-Hsin Yang [2*], Hsin-Ming Wu [3], Jia-Jing Lin [4], Shiau Jing Ho [5], Cheng-Nan Liu [6]

ABSTRACT

This paper presents a unique case of a detention pond within a freeway interchange ramp. A wrap-around geosynthetic-reinforced soil slope (RSS) backfilled with marginal soil was used as the waterfront retaining structure of the detention pond. In general, RSS with marginal backfill is considered unsuitable for waterfront structures because the infiltration or saturation may adversely affect the performance and stability of the slope. However, for this project, the short flooding duration and low permeability of the clayey backfill limited the saturated zone to the front face of the slope. Because the RSS is an internally stable structure, saturation of the front face does not affect the overall system stability. Details of the design and construction of the RSS are first discussed. A series of transient seepage and slope stability analyses were then performed to evaluate the effect of porewater pressure caused by flooding on the global stability of the RSS. Moreover, a hypotetical case involving critical conditions—a high phreatic surface in the reinforced zones and no external water in the detention pond (*i.e.,* drawdown conditions)—was analyzed. The project was completed in November 2015, and since then, the RSS in the detention pond has encountered more than 15 complete flooding and discharge cycles without any damage or observable deformation. This study demonstrated that RSS is a sustainable solution for infrastructure development that effectively balances safety, costs, ecological concerns and reduces waste, pollution, and CO_2 emissions.

Key words: Geosynthetic-reinforced soil slope, waterfront retaining system, flood detention pond, marginal backfill, sustainability.

1. INTRODUCTION

As in many other countries, in Taiwan, urbanization and climate change have caused stormwater runoff to become increasingly difficult to discharge through regional drainage systems. Therefore, detention ponds are necessary for sponge cities and low-impact development (LID). This paper presents a unique case of using a wrap-around geosynthetic-reinforced soil slope (RSS) as the waterfront retaining structure of the detention pond for flood control. This detention pond project is located within the northern ramp of the Shalu Interchange of National Freeway No. 3, west of Taichung, the second-largest city in Taiwan. Stormwater runoff collected in the catchment area has caused flooding in the downstream Shalu area in the past years. The Freeway Bureau decided to enlarge and deepen the original small detention pond in the Shalu Interchange to resolve the flooding problem.

This case is unique because the RSS was backfilled with locally available soil, with a fines content of approximately 65%,

and used in flood basin environments. Figure 1 displays the gradation limits for backfill suggested in the design guidelines (Elias *et al.* 2001; AASHTO 2002; Berg *et al.* 2009). Besides, the plasticity index (PI) of the backfill is specified (PI ≤ 6 and 20 for walls and slopes, respectively). The soil that satisfies the grain size recommendations specified in the design guidelines (*i.e.,* granular soil) is considered good quality backfill. In contrast, the soil that does not meet the grain size recommendations (*i.e.,* cohesive soil) is referred to as marginal backfill. Marginal backfill was adopted primarily because of economic and sustainability concerns, as explained in later sections.
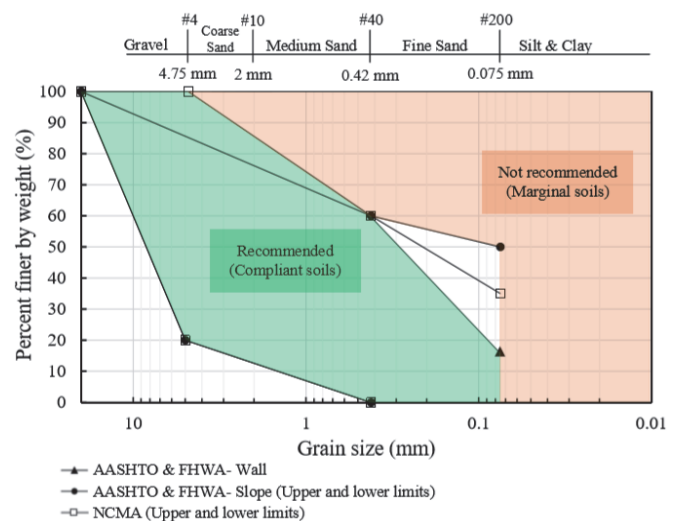

Fig. 1 Grain size distribution of backfill in GRS structures as recommended by design guidelines

Some successful cases of geosynthetic-reinforced soil (GRS) structures with marginal backfill have been reported; however, problems including considerable deformation or even failure have also been observed. The low draining capacity of fine soils could compromise the performance of reinforced soil structures upon wetting from rainfall infiltration or seepage due to the build-up of pore water pressure (PWP) within backfills (Zornberg and Mitchell 1994; Mitchell and Zornberg 1995; Yoo and Jung 2006; Valentine 2013; Koerner and Koerner 2013, 2018). Koerner and Koerner (2018) investigated 320 excessive deformation or failed cases of GRS structures. Statistical data revealed 73% of the failed cases were related to silt or clay as backfill, and 35% of the failures were caused by internal or external water. Therefore, the design and construction of GRS structures with marginal backfill should be carefully evaluated. Unlike good quality backfill, marginal soil cannot be considered a free-draining material. The effect of PWP induced by rainfall infiltration or seepage should be considered in stability analyses. In addition, proper quality control and inspection during construction and an adequate drainage system are essential to ensure the stability of GRS structures with marginal backfills (Christopher *et al.* 1998; Christopher and Stuglis 2005; Raja *et al.* 2012).

Few studies have investigated the performance of GRS structures in waterfront revetment and coastal protection. Yasuhara and Recio-Molina (2007) conducted model tests on geotextile wraparound revetments (GWRs) against wave action. The test results indicated the GWRs performed stably under wave action. The stability of the GWRs could be improved with simple modifications (*i.e.,* injecting seaward-facing GWRs with mortar and sewing reinforcement layers together). Their tests demonstrated that GRS walls used as waterfront structures are preferable for shoreline protection. Miyata *et al.* (2015) performed full-scale experiments to evaluate the performance of steel strip reinforced soil walls by transient flooding. The test walls were 6 m high and were flooded and drained to the midheight of the wall in four cycles. Their test results indicated that the reinforced soil walls performed well during the flooding and draining cycles. The flooding had a minor influence on the mobilized reinforcement tensile loads but substantially reduced the pullout capacity depending on the soil type.

Based on the discussion above, this paper presents a successful case of applying an RSS with marginal backfill as the retaining structure of a detention pond for flood control. This paper has the following objectives: (1) to introduce the selection, planning, design, and construction of the RSS of the detention pond; (2) to discuss the reasons for and concerns regarding the use of on-site

marginal soil as backfill in the flood basin environments; (3) to evaluate the stability and investigate the potential failure mechanism of the RSS under changing water levels; and (4) to discuss the performance and challenges of the RSS after the completion of the construction. The findings presented in this paper serve as a valuable and practical reference for RSS design for waterfront structures.

2.   PROJECT DESCRIPTION AND CONSIDERATIONS

2.1   Project Description and Subsurface Soil Conditions

The detention pond project is located within the northern ramp of Shalu Interchange on National Freeway No. 3 in the west of Taichung city, Taiwan. Figure 2 presents a satellite image of the project site. The new detention pond was constructed to replace the original one with insufficient storage capacity. Figure 3 presents an aerial photo of the original detention pond. The dimensions of the original detention pond are approximately 25 m × 15 m × 3 m (length × width × depth). Because of the insufficient storage capacity (only 1,125 m^3), the surface runoff collected in the catchment area (457,000 m^2) frequently caused the original flood detention pond to overflow, consequently causing flooding in the downstream Shalu area. Based on the hydrological analysis, the new required detention capacity is 20,632 m^3, 18.3 times larger than the original one. This capacity for the proposed enlarged and deepened detention pond was achieved by digging down from the original ground level. Figure 4 presents photos of the new heart-shaped flood detention pond. The proposed detention pond is meant to collect stormwater runoff from the catchment area, store it to prevent peak discharge, and then slowly discharge it to the downstream creek to resolve the flooding problem in the Shalu area. The delay time generated by the detention has been estimated to be 188 minutes from the peak.

Regarding the geological formation, the project site is located on the laterite terrace deposits of the upper Pleistocene Tokoshan formation. The subsurface strata consist mainly of cobble, gravel, and laterite (red clayey soil). The average thickness of the laterite terrace deposits is approximately 42 m. Figure 5 reveals the on-site materials typically exposed during the excavation process. The cobble and gravel layer was formed during the intense orogeny in Taiwan between 1.2 and 1.9 million years ago. It accumulated along the coastline of ancient Taiwan and then uplifted during the

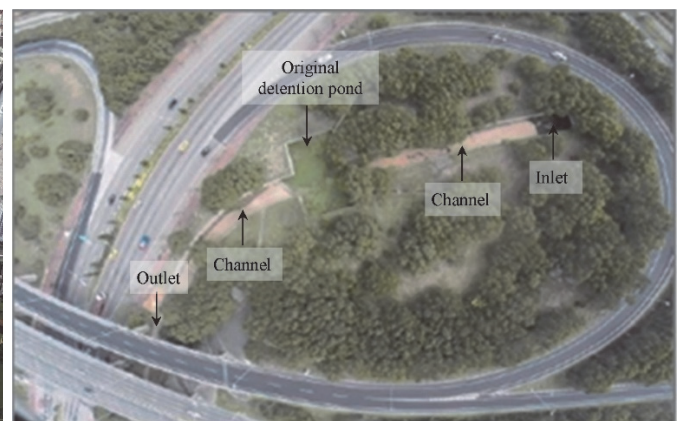**Fig. 2   Satellite image of the project site (from Google Earth)**

Fig. 3   Aerial photo of the original detention pond

(a) Aerial photo

(b) Panorama

Fig. 4　New heart-shaped detention pond

western orogeny over 550,000 years. The cobble and gravel are quartzite, with a round, oval shape. The cobble and gravel particle content is more than 70% in weight, with a particle size mostly greater than 30 mm and a maximum size of up to 400 mm. The cobble and gravel layer is cemented by clay, silt, and sand, but the cementing force for conglomeration is weak.

(a) Cobble and gravel are screened and piled aside

(b) Close view

Fig. 5　Typical onsite materials of the laterite terrace deposits exposed during construction excavation

The geotechnical investigation results indicated that the standard penetration test (SPT) values of the subsurface soil were higher than 50 (*i.e.,* SPT-N ≥ 50). The high SPT-N values are attributed to the presence of cobble and gravel. Groundwater was not observed under normal conditions, indicating that the groundwater is deeper than the borehole depth (~15 m). However, because the project is located in the slope area, with an average 10° downward gradient to the west, the groundwater level could rise because of seepage accumulated from the upland during storm events. Figure 6 shows the grain size distribution curve for the red clayey soil, containing 35% sand, 32% silt, and 33% clay. The behavior of the fine materials is controlled by the red clay, which has low permeability. The red clayey material has a liquid limit (LL) = 27 and a plasticity index (PI) = 12, as indicated by Atterberg limit tests, and is classified as low-plasticity clay (CL) according to the Unified Soil Classification System.
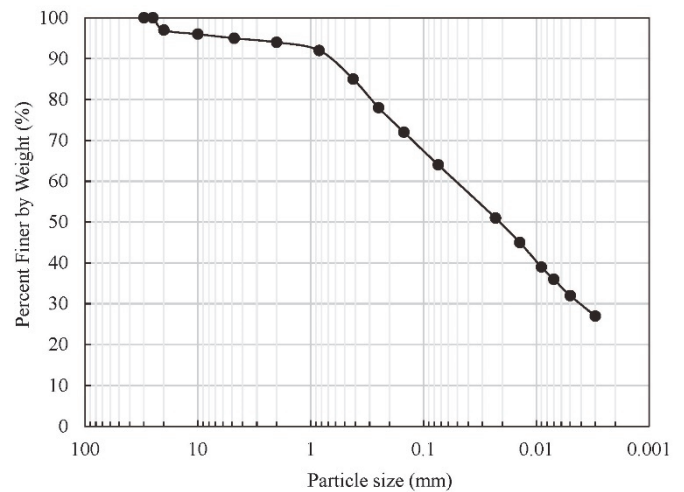

Fig. 6　Grain size distribution curve of the red clayey soil

2.2　Reasons for Using the On-Site Marginal Soil as Backfill

As discussed in the previous section, the on-site geological materials contain cobble, gravel, and red clayey soil. During the detention pond excavation, the excavated materials were screened

and classified. Because cobble and gravel are valuable for building construction, they were reserved for other construction projects after screening. The remaining red clayey soil was used as the backfill for the RSS and the base of the detention pond basin. According to the design guidelines (Elias *et al.* 2001; AASHTO 2002; Berg *et al.* 2009), the red clayey soil, containing approximately 65% fines, was classified as marginal backfill. The on-site clayey soil was used because of economic and sustainable considerations. Besides, the local regulation requires that excavated and backfilled soils be balanced at construction sites. Under Taiwan's environmental regulations, using soils outside construction sites is rather restricted, if not impossible. Environmental protection, pollution, and CO_2 emissions caused by transportation and traffic are vital concerns.

The success of many cases and experiences in Taiwan also supported using the on-site marginal soil as a backfill for the GRS structures. In past cases, marginal soil has been considered an alternate backfill when granular backfill was unavailable or too expensive or when borrowed materials may have had a negative environmental impact. Figure 7 presents four cases of RSS with on-site cohesive backfill. Figure 7(a) displays a 35-m RSS in a residential community used for slope stabilization. In 1993, it was the highest GRS structure in the world. Figure 7(b) displays a 30-m RSS at National Chi Nan University used for slope stabilization. Chou *et al.* (2020) conducted a detailed investigation of the sustainable renovation of this RSS. Figure 7(c) presents a 40-m RSS near Sun Moon Lake used for landslide remediation. Figure 7d displays a 25-m RSS in Tianliao Moon World used for slope protection and to prevent the breach of the uphill lake due to severe mudstone erosion. Because these RSSs were all backfilled with marginal soil, they were carefully designed and constructed with special attention to the drainage system. The evaluation of the slope stability considered the effect of PWP. These aspects are discussed in detail in later sections.

(a) A 35 m RSS of a residential community for slope stabilization, once the highest wall in the world in 1993
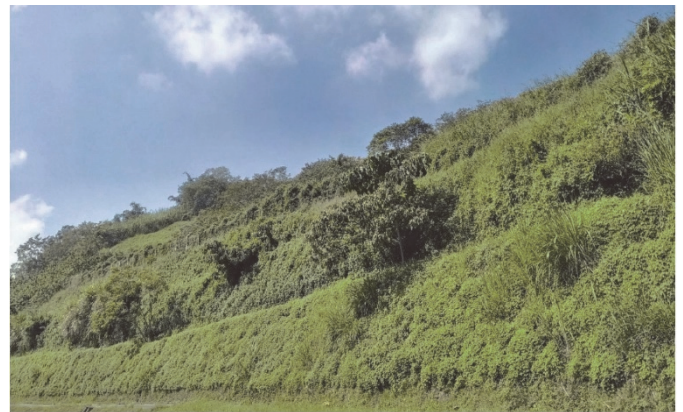
(b) A 30 m RSS at National Chi Nan University for slope stabilization

(c) A 40 m RSS near Sun Moon Lake for landslide remediation

(d) A 25 m RSS in Moon World for mudstone protection

Fig. 7   Geosynthetic-reinforced soil slope with onsite cohesive backfill in Taiwan

2.3   Selection of Earth Retaining System

Two types of earth retaining systems for the detention pond were evaluated under initial design: a conventional reinforced concrete (RC) wall and a wrap-around RSS. Many aspects are considered during the selection phase, including cost, appearance, safety, earthquake resistance, drainage system, ecology, landscape, and CO_2 emissions. Table 1 presents a comparison between the RSS and RC walls as discussed by Chou *et al.* (2018). RSS has considerable advantages over RC walls in the engineering life cycle. Because of these advantages, the RSS was selected as the retaining structure to protect the slopes of the new detention pond. The RSS was constructed in two tiers, with a slope ratio of 1 (V):0.5 (H) for each tier. Figure 8 illustrates a cross-section of the RSS across the basin of the detention pond. A RC wall with this design configuration could cost approximately US$478,200 more than would the RSS. Christopher (2014) also indicated that using GRS structures can reduce costs by 25% ~ 50% compared with the expense of RC structures and that using on-site marginal soil can reduce total wall costs by 20% ~ 30%. Table 2 lists the carbon footprint calculation of the RSS and RC wall for this project. The vegetated RSS used in this project could reduce CO_2 emission by an estimated 1213.92 tons compared with the RC wall.

Table 1   Comparison of the reinforced soil structure with reinforced concrete wall

Comparison item	RC walls	GRS structures
Cost	The cost is higher if the wall is taller than 5 m. Unit price increases significantly with height.	The cost is competitive if the wall height is lower than 5 m. If the wall is taller than 5 m, the price would be lower than the RC wall.
Appearance	Concrete surface.	Vegetated facing if wrap-around facing is adopted.
Design concept	External stability. Need a facing to resist bending moment.	Internal stability. Part of the lateral earth pressure is balanced by the friction between the reinforcement and adjacent soil.
Earthquake (EQ) resistance	Low EQ resistance. The concrete facing and soil have different periods and frequencies and may cause separation between them during strong earthquakes.	High EQ resistance. The reinforced material has strong tensile resistance; therefore, it can avoid tensile and shear cracks in the backfill. The soil and reinforcement composite has excellent seismic resistance, and the friction resistance may prevent the separation between reinforcement and surrounding soil. When using the wrap-around facing wall, because there is no concrete facade, the earthquake would not cause separation between the wall facade, connection, and backfill.
Ability to tolerate settlement	Generally, 5.0 cm is the maximum allowable settlement. Since the facade is rigid, only a tiny differential settlement is allowed.	A settlement of up to 30 cm is acceptable. Although the foundation soil may settle a substantial amount, the differential settlement can be reduced significantly due to the leveling effect of reinforcement. Besides, the use of preloading may eliminate the possibility of subsidence after construction.
Drainage system	The drainage layer and pipes are usually installed immediately behind the wall.	The drainage layer is installed between the backfill and the original soil and connected to the bottom to avoid softening of the backfill caused by seepage due to rainwater infiltration.
Carbon emission	Carbon dioxide emission is relatively large due to concrete/steel production, transportation, and wall construction.	Carbon dioxide emission is about 1/5 of the counterpart of RC wall. Additionally, if the wrap-around facing with vegetation is used, the plant photosynthesis can balance the carbon dioxide emitted. It may achieve carbon-neutral or even negative carbon emissions during the life cycle of the GRSW.

Table 2   Carbon footprint calculation by comparing the RSS and RC wall for this project

Comparison item	RC wall	RSS
Carbon emission (TCO$_2$e)	1348.33	194.45
Carbon reduction by facing vegetation (TCO$_2$e)	0	60.14
Net Carbon emission (TCO$_2$e)	1348.33	134.31
Difference between two retaining structures (TCO$_2$e)	1348.33 − 134.31 = 1213.92	

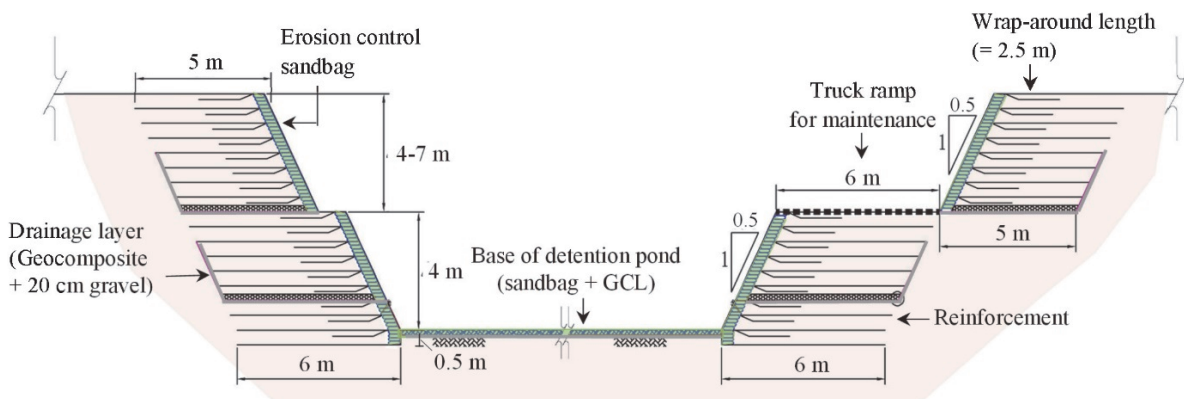Note: no vegetation on the concrete facing of the RC wall

Fig. 8   A typical cross-section of the geosynthetic-reinforced soil slope across the basin of the detention pond

2.4   Design and Construction of RSSs

The flood detention pond was constructed by excavating the ground to approximately 10 m (Figs. 4 and 5). The total excavation area was approximate 6,000 m², and the detention capacity was 20,632 m³. The detention pond has two inlets and two outlets. The two inlets discharge the stormwater runoff from the catchment area into the detention pond (Fig. 4). The two outlets are in the same position but at different elevations (Fig. 9). The upper outlet, located 5.75 m above the base of the detention pond, discharges the overflow of the flood into an open channel, thereby controlling the maximum water level in the detention pond at this elevation. The upper outlet functions as an emergency spillway to maintain the safety of the detention pond during storms. The lower outlet, located 0.75 m above the base, consists of three 100-cm-diameter drainage pipes. The lower outlet discharges the remaining flood-water in the detention pond and keeps the pond dry after storms.

An RSS was constructed to stabilize the excavated slope of the detention pond basin. The total length of the RSS is 285 m, and it surrounds the detention pond basin. Figure 8 presents the configuration of the RSS. The RSS is 8 to 11 m high and comprises two tiers. Each tier has a height ranging from 4 to 7 m, depending on the on-site topography, and the offset distance between the two tiers is 1 to 6 m. The significant offset distance (6 m) enables the RSS to serve as a downslope ramp for trucks, thus providing access for long-term maintenance (*i.e.,* dredging the deposited sediments as shown in Fig. 9). The slope face inclination ratio is 0.5 (H):1 (V) (~63°). The reinforcement is polyester (PET) geogrid, with an ultimate tensile strength of $T_{ult} = 180$ kN/m, determined through a single rib tensile test (ASTM D6637) (Fig. 10). The geogrid layers are 5 and 6 m long for the upper and lower tiers, respectively, spaced 0.5 m apart vertically. The slope face is formed by the geogrid wrapping around the sandbags (Fig. 11(a)). The length of the wrap-around (or secondary) reinforcement is 2.5 m. To prevent slack in the loopback section, the contractor pre-tensioned the reinforcement by pulling the wrap-around reinforcement tightly with a backhoe during construction. The sandbag for erosion control is made of high-durability erosion control mate. The size of the openings in the sandbag is less than 1.5 mm to prevent the erosion of the backfill material. The slope was vegetated through hydroseeding to create a green and natural appearance.

Compaction of the marginal backfill is essential. For field compaction, the soil was compacted using drum rollers (Fig. 11(b)) on every 30-cm soil lift, and the soil was required to reach 90% of maximum dry unit weight $\gamma_{d,max}$ according to the results of the modified Proctor compaction test. The backfill within 1 m of the slope face was compacted using vibratory plate compactors to prevent excessive facing displacement caused by the heavy compaction machine. During construction, the field density was inspected frequently for compaction control. A strong Typhoon Dujuan struck Taiwan in September 2015, which coincided with the construction process, and brought 93 mm of precipitation in 30 hours to the Shalu area. Because clayey soil cannot be easily dehydrated after being moistened, controlling the moisture content of backfill during typhoons and storms is crucial; soil compacted

Fig. 9   Detention pond with outlets, reinforced soil slope and downslope ramp for truck access
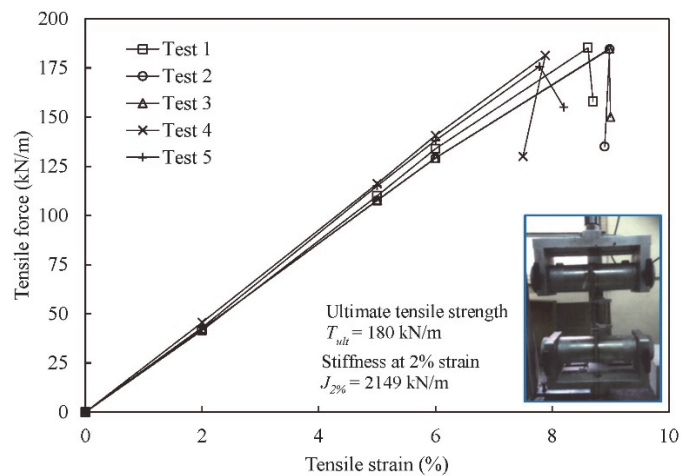

Fig. 10   Reinforcement single rib tensile test

| (a) Wrap-around facing | (b) Geogrid installation and compaction | (c) GCL at the base of the basin and covered with sandbags |

Fig. 11   Construction details

with high moisture content could increase the deformation and decrease the stability of a slope. Therefore, the backfill soil was covered with a waterproof tarpaulin during typhoons and storms to prevent rainfall infiltration. Water in the detention pond was diverted to protect the backfill from immersion (Fig. 12). The backfill was verified to have the appropriate moisture content for compaction before the construction resumed after the typhoon and storms.

Regarding the design of the drainage system, a drainage chimney was installed in each tier of the RSS (Fig. 8). The drainage layer consists of a geocomposite with 20 cm of gravel soil. The gravel was placed directly on top of the geocomposite and geogrid, a method that has been proven to accelerate PWP dissipation effectively. It increases the drainage capacity of the soil–geotextile system (Raisinghani and Viswanadham 2010; Thuo *et al.* 2015; Yang *et al.* 2018). Fine-grain soils also reduce surficial intrusion and long-term clogging in geotextiles (Lin and Yang 2014). Besides, it increases pullout resistance (Abdi and Zandieh 2014) and enhances reinforced soil strength and deformation characteristics by strengthening the soil–reinforcement interface (Unnikrishnan *et al.* 2002; Abdi *et al.* 2009; Yang *et al.* 2016, 2018). Finally, a blanket of geosynthetic clay liner (GCL), functioning as a hydraulic barrier, was placed at the base of the detention pond to prevent water leakage and mitigate the potential of uplift pressure acting on the adjacent highway foundation during flooding (Fig. 11(c)). The GCL was carefully installed and covered with sandbags to prevent penetration and breakage due to any sharp object or debris in the flood discharge.

Fig. 12   The site suffered by Typhoon Dujuan during construction

2.5   Concerns Regarding the Use of Marginal Backfill in Flood Basins

Although RSSs have been widely applied in slopes and other on-land projects, they are seldom used as waterfront structures. RSSs used in flood basin environments, especially backfilled with marginal soil, may raise concerns regarding the loss of matric suction, decrease in soil shear strength, and decrease in soil–reinforcement interaction when the soil is saturated. As a result, RSSs are rarely used in waterfront cases, and if used, the type of backfill would likely be limited to granular soils. Table 3 summarizes the advantages and disadvantages of using various backfills as waterfront retaining structures. Although clayey soil is considered marginal backfill in most design manuals or specifications, it is the superior option from economic and sustainability standpoints.

The first safety concern is that seepage flow caused by flooding may affect the stability of the RSS. Local hydrological data and field observations from storms indicated that the water level in the detention pond generally increased but then decreased at most for two days. During this short retention period, rainfall infiltration and flood seepage into the reinforced backfill are limited because the compacted red clayey soil has low permeability. This is supported by the numerical study of Yang *et al.* (2019b), which indicated that the PWP and factor of safety (FS) of RSSs with clayey backfill demonstrated no or slight variation during short rainfall events. In addition, Jayanandan and Viswanadham (2019) performed a series of numerical analyses to evaluate the applicability of various backfill soils for GRS walls and reported similar results. The low permeability of backfill soil with 40% fines limited rainfall infiltration to the reinforced zone; thus, a substantial portion of the rainfall directly became runoff.

In the present study, the saturated hydraulic conductivity of the backfill was determined through triaxial permeability tests (ASTM D5084). The red clayey soil specimen was remolded and compacted in accordance with the compaction requirement in the field. Accordingly, the average saturated hydraulic conductivity of the backfill determined through the tests was $k_s = 2.4 \times 10^{-11}$ m/s. With this low k_s value, the area potentially saturated by flood immersion could be limited to the slope-facing zone (Fig. 13). Notably, the saturation of the front face of the RSS has little influence on face stability because the slope face is protected by the sandbags and double reinforcement layers (primary and wrap-around geogrids). In addition, the saturation of the front face of the RSS would not jeopardize the overall stability because the RSS is an internally stabilized structure sustained through the mobilized reinforcement tensile force along the potential failure surface (Fig. 13). The finite element (FE) studies of Chou (1992), Chou and Wu

Table 3   Comparison of various backfills of reinforced soil structures used for detention pond

| Backfill type	Infiltration rate	Softening due to infiltration	Stability concerns	Environmental concerns	Cost
Red clayey soil (as current design)	Very low	Only in front-facing, less than 1 m	Low to moderate, need to check	Low	Low
Original ground soil (without screening)	Moderate	Infiltration rate will be high, so softening zone may be large	Low to moderate, need to check	Low	High
Granular material (discharge clayey soils, or borrow from outside)	Very high	Not affected	Not affected	If borrow material is used, it may result in waste generation, air pollution, CO_2 emission, *etc.*	Highest
Silt (an assumed situation, not applicable in this case)	Moderate to high	Moderate to serious	High (could be dangerous during the rapid drawdown)	N/A	N/A
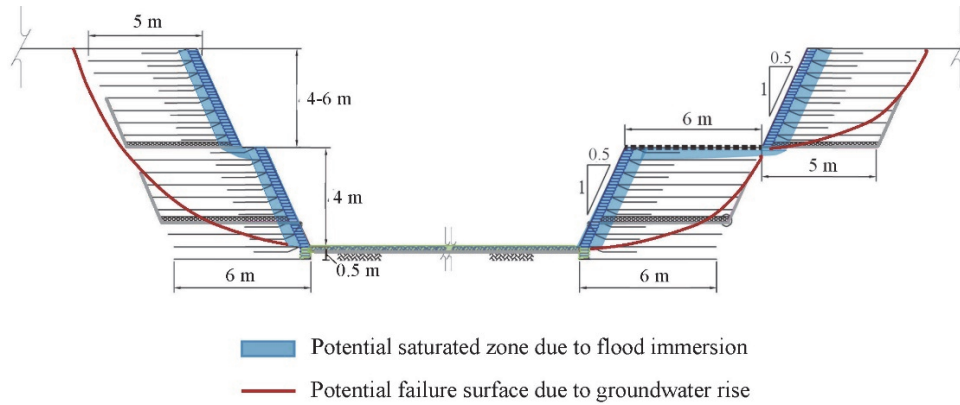
Fig. 13   **Illustration of the potential saturated zone due to flood immersion and the potential failure surface due to groundwater rise**

(1993), and Wu (2019) have demonstrated that the earth pressure of the backfill of GRS walls decreased gradually toward the face because the soil–reinforcement interaction balanced it and that the earth pressure approached to almost zero on the front face.

The second safety concern is that the rapid drawdown of the water level in the detention pond may cause slope failure. Riverbanks sometimes slide when the water level rapidly drops when excess PWP in the riverbank does not reduce simultaneously, causing soil shear failure. However, the flood detention time of the detention pool is short, and the seepage into the reinforced backfill is limited to a short distance (*i.e.,* the slope-facing zone). Therefore, the PWP in the reinforced backfill does not increase with the water level. Furthermore, the reinforcement provides tensile force (or apparent cohesion) to increase slope stability and the FS against slope failure. However, based on the authors' practical experience, precautions should be taken for silty soil backfill. Because the permeability of silt is higher than that of clay, its shear strength is lower than that of sand or gravel. Therefore, slope failure (especially rapid drawdown) could be a concern for short flooding and discharge cycles. This assertion is supported by the centrifuge test results and numerical simulation of Razeghi *et al.* (2019). They demonstrated that geogrid-reinforced soil walls backfilled with silty sand (containing 20% fines) failed within a few days after the occurrence of seepage because of the accumulation of excess PWP in the reinforced soil zone of the wall.

The third safety concern is that the water in the detention pond may affect the bearing capacity of the foundation of the RSS. The foundation soil comprises a layer of cobble and gravel (more than 70% in weight), considered a firm foundation. Although the foundation soil also contains 30% red clayey soil, it underwent a consolidation process during construction because of the overburden pressure applied by the RSS and the surcharge from the compaction. As a result, the void ratio of the red clayey soil decreased,

and the shear strength increased after the construction of the detention pond was completed. Therefore, the bearing capacity problem caused by water in the detention pond could be avoided.

3.   NUMERICAL ANALYSES

3.1   Numerical Model and Procedure

In addition to routine internal and external stability analyses (analyzing reinforcement breakage, pullout, sliding, overturning, and bearing capacity) of the RSS, a series of transient seepage analyses and slope stability analyses were performed using Geo-Studio (SEEP/W and SLOPE/W) to evaluate the influence of PWP caused by flood seepage on the global stability of the RSS. The PWP distribution and FS variation over time were investigated and discussed.

Figure 14 displays the numerical model and hydraulic boundary conditions. The numerical model was established in compliance with the configuration of the designed RSS, as shown on the left side of Fig. 8. The RSS model consists of 3,797 four-node quadrilateral elements. Fine mesh with a global height of approximately 0.1 m was designated for areas close to the slope-face that may be affected by flood seepage. A head boundary was prescribed for the slope-face (0 to 6 m above the basin base). Seepage boundaries were assigned to the right and left sides of the model to simulate the change in groundwater level during flooding. A closed (zero-flux) boundary was set on the bottom of the model. The potential seepage face review option was selected for the slope face, which can automatically switch the head boundary to a flux boundary when the water level decreases. This option also allows for the development of outward seepage force in the RSS to simulate rapid drawdown.
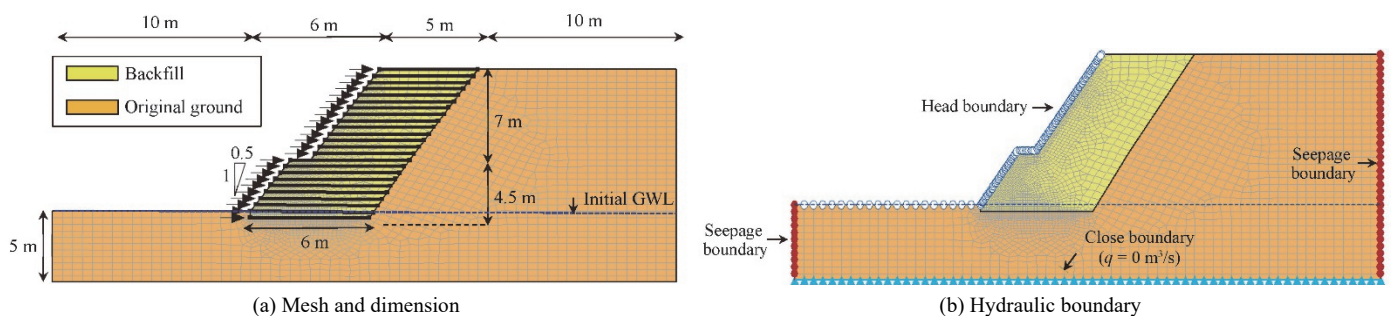

(a) Mesh and dimension

(b) Hydraulic boundary

Fig. 14   **Numerical model**

Figure 15 shows a flood history applied to the face of the RSS. The flood history was statistically derived using hydrological data from previous typhoons and storms (Table 4). The total flood period was 52 hours, and the water level on the slope face increased from the initial groundwater level to the maximum (6 m) during the first 2 hours. The water level remained maximum for 48 hours and returned to the initial groundwater level in the final 2 hours. The location of the initial groundwater level was assumed to be the bottom of the basin.

The flood history was applied to the upstream slope boundary in the transient seepage analysis. Each hydraulic head increment was 0.1 m, and the numerical convergence for each applied head increment was calculated. The limit equilibrium was calculated in slope stability analyses using Spencer's method (Spencer 1967), satisfying all equilibrium conditions. A circular failure surface was assumed in the analysis. The PWP predicted using SEEP/W was automatically transferred to SLOPE/W as the input porewater pressure to calculate the effective stress at a given time.

3.2   Input Soil and Reinforcement Properties

Table 5 lists the input soil and reinforcement parameters. The soil shear strength parameters and saturated hydraulic conductivity
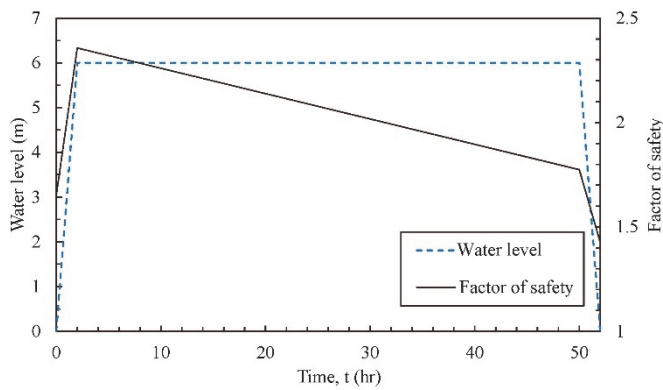
Fig. 15   Time history of water level and variation of FS with time

Table 4   Summary of rainfall data in the project area caused by typhoon and storm events

No.	Rainfall events	Starting Date (YYYY-MM-DD)	Accumulated precipitation (mm)	Maximum rainfall per hour (mm)	Duration (hr)
1	Typhoon Dujuan	2015-09-28	93.0	16.0	30.5
2	Typhoon Malakas	2016-09-17	43.5	7.5	25
3	Typhoon Megi	2016-09-27	88.5	8.5	28
4	Heavy rain	2017-06-01	145.0	12.0	60
5	Heavy rain	2017-06-14	475.0	29.5	111
6 &7	Typhoon Nesat and Haitang	2017-07-29	235.0	32.5	33
8	Heavy rain	2018-08-23	168.5	27.0	52
9	Heavy rain	2019-05-17	157.0	55.5	81
10	Heavy rain	2019-06-10	158.0	30.5	61
11	Typhoon Lekima	2019-08-09	160.5	61.0	30
12	Heavy rain	2019-08-10	333.5	26.0	183
13	Heavy rain	2020-05-21	94.5	10.5	37
14	Typhoon Hagupit	2020-08-02	88.0	50.0	22
15	Tropical storm Choi-wan	2021-06-04	132.5	27.5	44

Note: the rainfall effects of Typhoon Nesat and Typhoon Haitang are combined because these two typhoons arrived in Taiwan one after another.

were obtained through the experimental tests in this study. The soil specimens were remolded and prepared with $\gamma_{d,\max} = 17.5$ kN/m³, and an optimal moisture content of $\omega_{opt} = 12\%$, as determined through the modified Proctor compaction tests. A series of direct shear tests (ASTM D3080) with a slow shearing rate was performed to determine the shear strength parameters of the backfill. The soil specimens were saturated and immersed in the water for two days to simulate the flood basin environments. Based on the test results obtained under soil saturation conditions, the shear strength properties of the backfill were effective friction angle (ϕ') = 23.7° and effective cohesion (c') = 21 kPa. The substantial amount of effective cohesion may have been due to the over-consolidation of the soil caused by compaction.

The saturated hydraulic conductivity of the backfill was determined through triaxial permeability tests (ASTM D5084). After the specimens were consolidated in the consolidation phase, a back pressure difference of 20 kPa was introduced to the specimens, and the outflow discharge driven by the pressure difference was measured using a volume gauge. The soil's hydraulic conductivity was then calculated using Darcy's law. The average saturated hydraulic conductivity of the backfill determined through the tests was $k_s = 2.4 \times 10^{-11}$ m/s. However, the numerical analyses using such low k_s value show almost no water advances from the slope face into the backfill during the period of the applied flood history. This k_s value is increased by one order (*i.e.*, $k_s = 2.4 \times 10^{-10}$ m/s) in the numerical analyses in order to observe a clear seepage advancement. The rationales for increasing k_s value is because the soil field density may not be well controlled compared to the lab tests. In addition, the backfill in the field may contain a few stones. These stones may increase the soil permeability in the field, but these stones were removed for the permeability test in the laboratory. Many studies have revealed that hydraulic conductivity determined in the laboratory is typically lower than that obtained in the field (Oh and Lu 2015; Gribb *et al.* 2004; Benson *et al.* 1997).

The soil in the original ground layer consists of more than 70% cobble and gravel. The unit weight of the cobble–gravel layer was $\gamma = 20.5$ kN/m³. The soil shear strength parameters and saturated hydraulic conductivity were adopted from the field test results, as documented in the local site investigation reports. The soil shear strength properties of the cobble–gravel layer were $\phi' = 40°$ and $c' = 5$ kPa, determined through the large-scale in situ direct

Table 5   Input soil and reinforcement parameters

Properties	Value
Backfill (Red clayey soil)	
Unit weight, γ (kN/m³)	19.6
Maximum dry unit weight, γ_d (kN/m³)	17.5
Optimal water content, ω_{opt} (%)	12
Cohesion, c' (kPa)	21
Friction angle, ϕ' (°)	23.7
Saturated hydraulic conductivity, k_s (m/s)	2.4×10^{-10}
Original ground layer	
Unit weight, γ (kN/m³)	20.5
Cohesion, c' (kPa)	5
Friction angle, ϕ' (°)	40
Saturated hydraulic conductivity, k_s (m/s)	5×10^{-4}
Reinforcement	
Ultimate tensile strength, T_{ult} (kN/m)	180
Long-term tensile strength, T_{al} (kN/m)	25.7
Long-term strength reduction factor, RD	7
Interface efficiency factor, E_{inter}	0.5

shear test. The saturated hydraulic conductivity of the cobble–gravel layer was $k_s = 5 \times 10^{-4}$ m/s, which was derived from the field pumping tests.

The reinforcement had an ultimate tensile strength of $T_{ult} = 180$ kN/m, obtained through a single rib tensile test (ASTM D6637) as shown in Fig. 10. Because the marginal soil was used as backfill, according to the suggestions in the design guidelines (Berg *et al.* 2009; Elias *et al.* 2001), a high reduction factor ($RD = 7$) should be applied to account for the long-term strength reduction due to installation damage, durability, and creep. Therefore, the long-term reinforcement tensile strength used in the numerical analyses was $T_{al} = 25.7$ kN/m ($= 180/7$). The interface efficiency factor was adopted to calculate the soil–geogrid interface shear strength parameters (c_a' and δ') as follows:

$$E_{\text{inter}} = \frac{c_a'}{c'} = \frac{\tan\delta'}{\tan\phi'} \tag{1}$$

where E_{inter} is the interface efficiency factor; c_a' and c' are the interface and soil cohesion, δ' and ϕ' are the interface and soil friction angle, respectively. Based on experimental studies on the soil-geogrid interface, $E_{\text{inter}} = 0.5$ was used for the numerical analyses (Koutsourais *et al.* 1998; Abu-Farsakh *et al.* 2007; Esmaili *et al.* 2014; Hatami and Esmaili 2015). A low E_{inter} value accounted for the substantial reduction in interface strength for marginal soils under saturated conditions compared with those under as-compacted conditions, as reported in the literature mentioned above. Figure 16 illustrates the input tensile force distribution along the reinforcement length, which was incorporated into the equilibrium equation (balance of forces or moments) as the stabilizing forces in the slope stability analysis. The bilinear tensile force distribution along the reinforcement length was input according to its ability to provide rupture and pullout resistance. The rupture resistance was calculated based on the input reinforcement tensile strength (*i.e.,* T_{al}), while the pullout resistance was determined using the pullout equation.

$$P_r = R_c L_e \left(c_a' + \sigma_v' \tan\delta' \right) \tag{2}$$

where P_r is the pullout resistance; R_c ($= 2$) is the coverage ratio (or surface area factor), considering both the top and bottom surfaces of reinforcement. Besides, L_e is the horizontal distance to the free end of reinforcement; c_a' and δ' are the interface cohesion and friction angle, respectively, σ_v' is the effective overburden pressure on the reinforcement layer. The pullout resistance of the reinforcement increased linearly from zero at the free end of the reinforcement to a value equal to the input reinforcement tensile strength (Fig. 16).
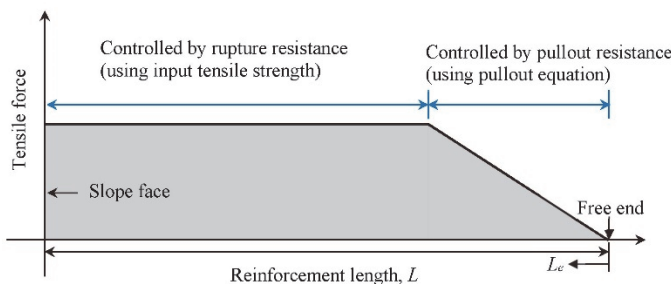

Fig. 16   Schematic of input tensile force distribution along reinforcement length

3.3   Results and Discussion

Figure 17 presents the variation in the phreatic surface over time. The numerical results indicated that the maximum seepage infiltration distance in the reinforced zone was limited to approximately 60 cm because of the low permeability of the compacted red clay. Therefore, the area that could be saturated by flood immersion was limited to within 1 m of the slope face during the applied flood event. The numerical results verified the discussion on the safety of the RSS in Section 2.5. Notably, the variation in the phreatic surface in the original ground layer (*i.e.,* the soil layer behind the RSS) was associated with the changes in water level. The difference between the changes in the phreatic surface in the reinforced zone and the original ground could be attributed to the significant difference in permeability.
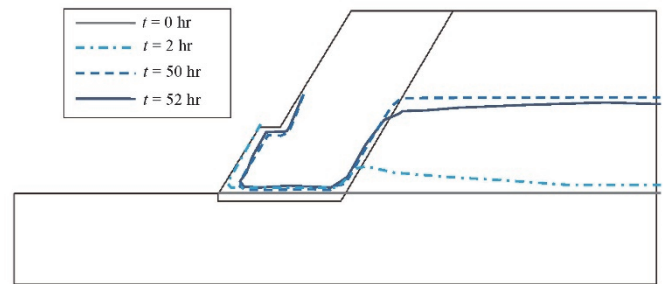

Fig. 17   Variation of phreatic surface with time

Figure 15 displays the change in FS over time, and Fig. 18 presents the numerical results (*i.e.,* FS and potential failure surface) at the selected times. The numerical results indicated that FS could change over time but that the RSS remained stable (FS > 1) throughout the flood event. At initial condition $t = 0$ h, FS was equal to 1.65 (Fig. 18(a)). When the water level was at maximum ($t = 0$-2 h), FS increased to 2.35 due to the imbalance in PWP between the front and the rear of the RSS (Fig. 18(b)). As shown in Fig. 18(b), the PWP in front of the RSS was higher than that at the rear of the RSS. This difference in pressure results in a resultant inward force acting on the slope face as a stabilized force, thereby increasing system stability. When the water level remained at maximum for two days ($t = 2$-50 h), the FS decreased to 1.77 as the seepage infiltration proceeded (Fig. 18(c)). Although the phreatic surface in the original ground rose to the maximum water level during this period, the system stability remained satisfactory because the cobble and gravel in the original ground layer had high soil shear strength. When the water level dropped to the initial level ($t = 50$-52 h), the FS decreased to 1.42, the minimum FS value during the flood event. The decrease in FS was caused by the imbalance in PWP between the front and the rear of the RSS (Fig. 18(d)). During this period, the water level in front of the RSS drained completely, whereas the PWP at the rear of the RSS dissipated relatively slowly. This difference in pressure causes an outward seepage force to act as a driving force, therefore decreasing system stability.

The potential failure surface exhibited a compound failure mode in which the failure surface partially cut through the reinforced zone and passed through the original ground layer. Despite the change in FS over time, the potential failure surface remained at a similar location throughout the flood event. The compound failure model has been reported as common failure modes for GRS
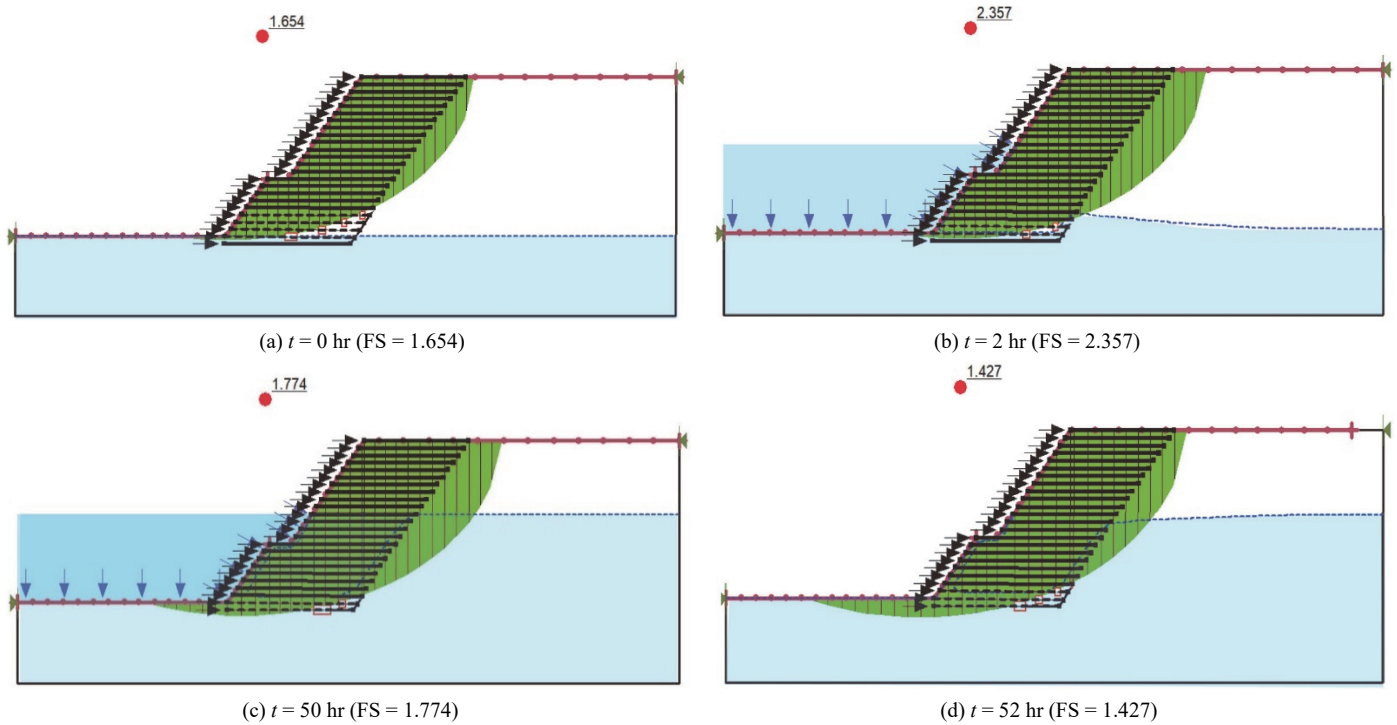
(a) $t = 0$ hr (FS = 1.654)

(b) $t = 2$ hr (FS = 2.357)

(c) $t = 50$ hr (FS = 1.774)

(d) $t = 52$ hr (FS = 1.427)

Fig. 18   Potential failure surface and FS at different timing

structures with marginal backfill under heavy rainfall in several failure case histories (Yoo and Jung 2006; Liu *et al.* 2012; Yang *et al.* 2019a).

In addition to these analyses, a hypothetical case involving a high phreatic surface in the reinforced zones and no external water in the detention pond was analyzed (*i.e.,* drawdown conditions; Fig. 19). In reality, this hypothetical case is unlikely to occur because the numerical results revealed that the water level in the detention pond must remain at a maximum for approximately 250 days for the phreatic surface in the reinforced zone to rise to a high level. However, no typhoon or storm event on record in Taiwanese meteorological data has lasted for such a long period. Nevertheless, this hypothetical case was analyzed to evaluate the stability of the RSS under the most extreme conditions. The numerical results indicated that the RSS had adequate FS (= 1.25) under these conditions (Fig. 19). An FS value of 1.1 is required in local codes for retaining walls or engineered slopes under storm conditions.
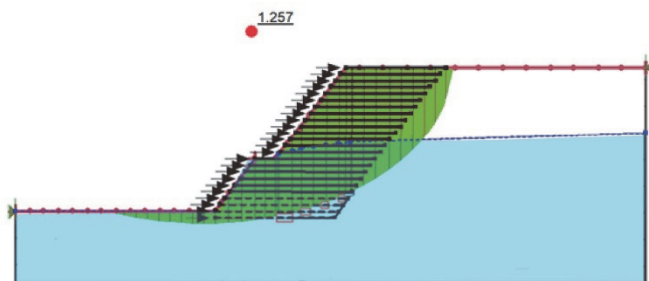

Fig. 19   Potential failure surface and FS at the assumed most critical conditions (FS = 1.257 at high groundwater level and rapid drawdown conditions)

4.   PERFORMANCE AND ACHIEVEMENTS

The RSS and flood detention basin construction was completed in less than 5 months, and the project was completed in November 2015. Figure 4 displays the finished project. Since the project was completed, the site has experienced many typhoon and storm events. Table 4 presents the rainfall data in the project area caused by these events. Figure 20 displays the performance of the GRS detention pond during a storm event. As expected, muddy water from upstream was temporarily deposited in the detention basin and then diverted smoothly to the downstream discharge area. The RSS used in flood basin environments has been thoroughly tested, and it exhibited neither damage nor observable deformation.

A remote sensing technique based on persistent scatterer interferometric synthetic aperture radar (PSInSAR) was used to measure the changes in land surface altitude in the project area. This study analyzed 2016 ~ 2020 data from Sentinel-1A, an earth-orbiting satellite, to determine the surface deformation of the RSS and surrounding area (Fig. 21). Figure 21(b) presents the displacement trends with time of the selected points near the RSS. Although the PSInSAR data may exist fluctuations which are the noise from measurement, the average ground displacement rate in vicinity of the RSS was negligible, less than 5 mm/yr over the analyzed period from 2016 to 2020. The satisfactory performance of the RSS indicated by the field observations and PSInSAR data suggests that RSSs with marginal backfill can be applied to waterfront structures if special attention and precautions are taken in design and construction. In addition, the detention pond functions well and thus resolves the flooding problem; no further flooding occurred in the city downstream after the project was completed.
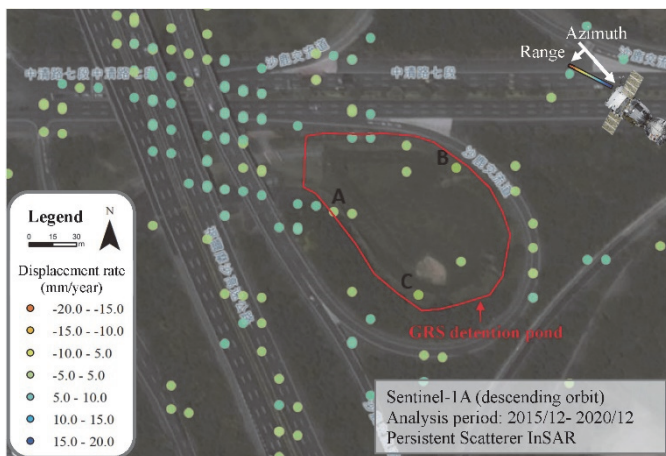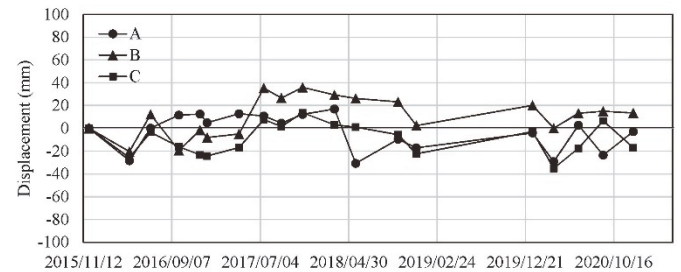
(a) Maintain stability under high water level

(b) Muddy water from the upstream watershed was temporarily deposited in the detention pond

Fig. 20   Performance of the GRS detention pond during a storm event

(a) PSInSAR data points

(b) Displacement *vs.* time of the selected points near the RSS

Fig. 21   PSInSAR data of the surface deformation of the RSS and surrounding area

In addition to demonstrating the construction's successes, the satisfactory performance during floods, and the RSS's disaster-mitigating capabilities, this study revealed that the RSS is a sustainable solution for infrastructure development. Because of global warming, sustainability in the lifecycle of infrastructure has received increasing attention during project development. Liu (2020) and Liu *et al.* (2021) selected 10 key indicators, namely risk mitigation and reliability, ecology, CO_2 emissions reduction, energy saving, waste reduction, durability, benefit and function, landscape, humanities and culture preservation, and creativity, to create a reliable method to evaluate the sustainability of civil infrastructure. Wrap-around, vegetated reinforced soil slopes are considered a typical sustainable green civil engineering structure (Chou *et al.* 2020; Taipei Civil Engineers Association 2004). The project fully utilized the on-site marginal soil to achieve the multiple benefits of sustainability, contributing to a circular economy, conserve resources and energy, reduce waste and CO_2 emissions, and create a biodiverse environment without using outside soil materials. The vegetated, wrap-around facing of the RSS also provides an eco-friendly environment for vegetation and animals, and the detention pond suits the surrounding topography and ramp nicely (Fig. 4(b)).

This project received the 2019 Excellence in Engineering Environment and Beautification Award from the Chinese Institute of Civil and Hydraulic Engineering in Taiwan. The project received the award because it was the first successful application of an RSS in flood detention, which represents both an academic and practical breakthrough. In addition, the full utilization of an existing interchange to minimize land use, the use of on-site materials to prevent environmental impact, the successful resolution of the downstream flooding problem, the preservation of the ecological environment and landscape, and the reduction of CO_2 emissions are achievements recognized by this award.

5.   CONCLUSIONS

RSSs have been successfully applied in various geotechnical projects for more than 30 years. However, concerns may arise regarding their use in waterfront projects, such as detention ponds, riverbanks, sponge cities, and low-impact development, especially when marginal soils are used as backfill materials. The potential infiltration and saturation of clayey backfill usually prompts concerns regarding safety because of the loss of matric suction, decrease in soil shear strength, and decrease in soil–reinforcement interaction.

This paper presents a unique case in which an RSS with marginal clay backfill was successfully used in a flood detention pond. The RSS can maintain its stability during short periods of flooding

and discharge because of its low permeability. The saturation of the slope front face does not affect the overall stability because the RSS is an internally stabilized structure. This project was completed in November 2015, and since then, the RSS in the detention pond has encountered more than 15 flooding and discharge cycles. Therefore, the RSS has been thoroughly tested and has demonstrated its integrity by exhibiting neither damage nor observable deformation.

A series of transient seepage and slope stability analyses were performed to evaluate the effect of PWP caused by flooding on the global stability of the RSS. The numerical results indicated that the maximum seepage infiltration distance in the reinforced zone was within 1 m from the slope-facing zone during the flood event. The FS values changed over time, but the RSS remained stable (FS > 1) throughout the flood event. The RSS exhibited an adequate FS (= 1.25) even under extreme conditions: a high phreatic surface in the reinforced zones and no external water in the detention pond (*i.e.,* drawdown conditions). In addition to providing the results of the stability analyses, this paper details the construction of the wrap-around facing, drainage system, compaction control, and hydraulic barrier layer at the bottom of the basin.

This study demonstrated that the RSS is a sustainable solution for infrastructure development that effectively balances safety, costs, waste and pollution reduction, CO_2 emissions reduction, and environmental protection. This project expanded the applicability of RSS to waterfront structures. It demonstrated the effectiveness of using marginal soil as a backfill, thereby eliminating the necessity of borrowing outside granular materials while protecting the environment and contributing to the circular economy.

ACKNOWLEDGEMENTS

DATA AVAILABILITY

The data and/or computer codes used/generated in this study are available from the corresponding author on reasonable request.

CONFLICT OF INTEREST STATEMENT

The authors declare that there is no conflict of interest.

NOTATION LIST

Symbols

c'	cohesion (kN/m^2)
c_a'	interface and soil cohesion (kN/m^2)
E_{inter}	interface efficiency factor
$J_{2\%}$	reinforcement stiffness at 2% strain (kN/m)
k_s	saturated hydraulic conductivity (m/s)
L_e	horizontal distance to the free end of reinforcement (m)

P_r	pullout resistance (kN/m)
R_c	coverage ratio
RD	reduction factor
q	discharge (m^3/s)
t	time (hr)
T_{al}	long-term reinforcement tensile strength (kN/m)
T_{ult}	ultimate tensile strength (kN/m)
γ	unit weight (kN/m^3)
γ_d	dry unit weight (kN/m^3)
$\gamma_{d,\max}$	maximum dry unit weight (kN/m^3)
δ'	interface friction angle (°)
ϕ'	friction angle (°)
σ_v'	effective overburden pressure (kN/m^2)
ω_{opt}	optimal moisture content (%)

Abbreviations

AASHTO	American Association of State Highway and Transportation Officials
ASTM	American Society for Testing and Materials
CL	Low plasticity clay
EQ	earthquake
FS	factor of safety
GCL	geosynthetic clay liner
GRS	geosynthetic-reinforced soil
GWR	geotextile wrap-around revetment
LID	low-impact development
LL	liquid limit
PET	polyester
PI	plasticity index
PSInSAR	persistent scatterer interferometric synthetic aperture radar
PWP	porewater pressure
RC	reinforced concrete
RSS	reinforced soil slope
SPT	standard penetration test

REFERENCES

AASHTO (2002). *Standard Specifications for Highway Bridges*. Officials, Seventeenth Edition, American Association of State Highway and Transportation Washington, DC.

Abdi, M.R., Sadrnejad, A., and Arjomand, M.A. (2009). "Strength enhancement of clay by encapsulating geogrids in thin layers of sand." *Geotextiles and Geomembranes*, **27**(6), 447-455. https://doi.org/10.1016/j.geotexmem.2009.06.001

Abdi, M.R. and Zandieh, A.R. (2014). "Experimental and numerical analysis of large-scale pull-out tests conducted on clays reinforced with geogrids encapsulated with coarse material." *Geotextiles and Geomembranes*, **42**(5), 494-504. https://doi.org/10.1016/j.geotexmem.2014.07.008

Abu-Farsakh, M., Coronel, J., and Tao, M.J. (2007). "Effect of soil moisture content and dry density on cohesive soil-geosynthetic interactions using large direct shear tests." *Journal of Material in Civil Engineering*, ASCE, **19**(7), 540-549. https://doi.org/10.1061/(ASCE)0899-1561(2007)19:7(540)

ASTM D3080. *Standard Test Methods for Direct Shear Test of Soils under Consolidated Drained Conditions*. ASTM International, West Conshohocken, PA, USA.

ASTM D5084. *Standard Test Methods for Measurement of Hydraulic Conductivity of Saturated Porous Materials using a*

Flexible Wall Permeameter. ASTM International, West Conshohocken, PA, USA.

ASTM D6637. *Standard Test Methods for Determining Tensile Properties of Geogrids by the Single or Multi-Rib Tensile Test*. ASTM International, West Conshohocken, PA, USA.

Benson, C.H., Gunter, J.A., Boutwell, G.P., Trautwein, S.J., and Berzanskis, P.H. (1997). "Comparison of four methods to assess hydraulic conductivity." *Journal of Geotechnical and Geoenvironmental Engineering*, ASCE, **123**(10), 929-937. https://doi.org/10.1061/(ASCE)1090-0241(1997)123:10(929)

Berg, R.R., Christopher, B.R., and Samtani, N.C. (2009). *Design of Mechanically Stabilized Earth Walls and Reinforced Soil Slopes*. FHWA, Washington, DC, Report No. FHWANHI-10-024.

Chou, N.N.S. (1992). *Performance of Geosynthetic-Reinforce Soil Walls, Doctoral Dissertation*. Department of Civil and Environmental Engineering, University of Colorado. https://doi.org/10.1680/gein.9.0228

Chou N.N.S. (1994). "A 35m high geogrid-reinforced slope: New heights and innovative construction." *5th International Conference on Geotextiles, Geomembranes and Related Products*, Singapore.

Chou, N.N.S., Liu, T.Y., Chen, P.H., Fan, C.C., and Zhang, J. (2020). "Failure investigation and sustainable renovation for slope at National Chi Nan University, Taiwan." *Journal of Performance of Constructed Facilities*, ASCE, **34**(5), 04020085. https://doi.org/10.1061/(ASCE)CF.1943-5509.0001459

Chou, N.N.S. and Wu, J.T.H. (1993). *Investigating Performance of Geosynthetic Reinforced Soil Walls*, Report No. CDOT-DTD-93-21, Colorado Department of Transportation.

Chou, N.N.S., Liu, T.Y., Chen, Y.S., and Cheng, H.C. (2018). "Comparison of various types of MSE wall facings." *11th International Geosynthetics Conference*, Seoul, Korea

Chou, N.N.S., Yang, K.H., Barrett, B., Wu, H.M., and Liu, T.Y. (2020). "Sustainable characteristics of reinforced soil structures – From ancient Great Walls to modern GRS walls." *Transportation Infrastructure Geotechnology*, **7**(3), 445-460. https://doi.org/10.1007/s40515-020-00121-y

Christopher, B.R. (2014). "Cost savings by using geosynthetics in the construction of civil works projects." *Proceedings of the 10th International Conference on Geosynthetics, 10ICG*, Berlin, Germany.

Christopher, B.R. and Stuglis, R.S. (2005). "Low permeable backfill soils in geosynthetics reinforced soil wall: State of the practice in North America." *Proceedings of North American Geo-synthetics Conference* (NAGS 2005), Las Vegas, Nevada, USA, GRI-19, 14-16.

Christopher, B.R., Zornberg, J.G., and Mitchell, J.K. (1998). "Design guidance for reinforced soil structures with marginal soil backfills." *Proceedings of the Sixth International Conference on Geosynthetics*, Atlanta, Georgia, **2**, 797-804.

Elias, V., Christopher, B.R., and Berg, R. (2001). *Mechanically Stabilized Earth Walls and Reinforced*. National Highway Institute, Federal Highway Administration.

Esmaili, D., Hatami, K., and Miller, G.A. (2014). "Influence of matric suction on geotextile reinforcement-marginal soil interface strength." *Geotextiles and Geomembranes*, **42**(2), 139-153. https://doi.org/10.1016/j.geotexmem.2014.01.005

Federal Highway Administration, (2009). *Design and Construction of Mechanically Stabilized Earth Walls and Reinforced Soil Slopes*, U. S. Department of Transportation Publication No. FHWA-NHI-10-024.

Gold-Joint Industry Co., Ltd., (2020). *Green Engineering Project Reports* (in Chinese).

Gribb, M.M., Kodesova, R., and Ordway, S.E. (2004). "Comparison of soil hydraulic property measurement methods." *Journal of Geotechnical and Geoenvironmental Engineering*, ASCE, **130**(10), 1084-1095. https://doi.org/10.1061/(ASCE)1090-0241(2004)130:10(1084)

Hatami, K. and Esmaili, D. (2015). "Unsaturated soil-woven geotextile interface strength properties from small-scale pullout and interface." *Geosynthetics International*, **22**(2), 161-172. https://doi.org/10.1680/gein.15.00002

Jayanandan, M. and Viswanadham, B.V.S. (2019). Geogrid reinforced soil walls with marginal backfills subjected to rainfall: A numerical study." *Indian Geotechnical Journal*, **50**(2), 238-251. https://doi.org/10.1007/s40098-019-00396-0

Koerner, R.M. and Koerner, G.R. (2013). "A database, statistics and recommendations regarding 171 failed geosynthetic-reinforced mechanically stabilized earth (MSE) walls." *Geotextiles and Geomembranes*, **40**, 20-27. https://doi.org/10.1016/j.geotexmem.2013.06.001

Koerner, R.M. and Koerner, G.R. (2018). "An extended data base and recommendations regarding 320 failed geosynthetic reinforced mechanically stabilized earth (MSE) walls." *Geotextiles and Geomembranes*, **46**(6), 904-912. https://doi.org/10.1016/j.geotexmem.2018.07.013

Koutsourais, M., Sandri, D., and Swan, R. (1998). "Soil interaction characteristics of geotextiles and geogrids." *Proceedings of the Sixth International Conference on Geosynthetics*, Atlanta, Georgia, **2**, 739-744

Lin, C.-Y. and Yang, K.-H. (2014). "Experimental study on measures for improving the drainage efficiency of low-permeability and low-plasticity silt with nonwoven geotextile drains." *Journal of the Chinese Institute of Civil and Hydraulic Engineering*, **26**(2), 71-82 (in Chinese). https://doi.org/10.1016/j.asej.2021.03.012

Liu, C.-N., Yang, K.-H., Ho, Y.-H., and Chang, C.-M. (2012). "Lessons learned from three failures on a high steep geogrid-reinforced slope." *Geotextiles and Geomembranes*, **34**, 131-143. https://doi.org/10.1016/j.geotexmem.2012.05.003

Mitchell, J.K. and Zornberg, J.G. (1995). "Reinforced soil structures with poorly draining backfills." Part II: case histories and applications. *Geosynthetics International*, **2**(1), 265-307. https://doi.org/10.1680/gein.2.0011

Miyata, Y., Bathurst, R.J., Otani, Y., Ohta, H., and Miyatake, H. (2015). "Influence of transient flooding on steel strip reinforced soil walls." *Soils and Foundations*, **55**(4), 881-894. https://doi.org/10.1016/j.sandf.2015.06.018

Oh, S. and Lu, N. (2015). "Slope stability analysis under unsaturated conditions: case studies of rainfall-induced failure of cut slopes." *Engineering Geology*, **184**, 96-103. https://doi.org/10.1016/j.enggeo.2014.11.007

Raisinghani, D.V. and Viswanadham, B.V.S. (2010). "Evaluation of permeability characteristics of a geosynthetic-reinforced soil through laboratory tests." *Geotextiles and Geomembranes*, **28**(6), 579-588. https://doi.org/10.1016/j.geotexmem.2010.01.001

Raja, J., Dixon, N., Frost, M., and Zornberg, J.G. (2012). "Designing with marginal fills: understanding and practice." *Proceedings of the 5th European Geosynthetics Congress*, 460-465.

Razegi, H.Z., Viswanadhamb, B.V.S., and Mamaghaniana, J. (2019). "Centrifuge and numerical model studies on the behaviour of geogrid reinforced soil walls with marginal backfills with and without geocomposite layers." *Geotextitles and*

Geomembranes, **47**, 671-684.
https://doi.org/10.1016/j.geotexmem.2019.103470

Spencer, E. (1967). "A method of analysis of the stability of embankments assuming parallel inter-slice forces." *Geotechnique*, **24**(4), 661-665.
https://doi.org/10.1680/geot.1967.17.1.11

Taipei Civil Engineers Association, (2004). *Guidelines for Design and Construction of Reinforcement Soil Retaining Structures in Integration with Ecology and Landscape.*

Thuo, J.N., Yang, K.-H., and Huang, C.-C. (2015). "Infiltration into unsaturated reinforced slopes with nonwoven geotextile drains sandwiched in sand layers." *Geosynthetics International,* **22**(6), 457-474.
https://doi.org/10.1680/jgein.15.00026

Unnikrishnan, N., Rajagopal, K., and Krishnaswamy, N.R. (2002). "Behaviour of reinforced clay under monotonic and cyclic loading." *Geotextiles and Geomembranes*, **20**(2), 117-133.
https://doi.org/10.1016/S0266-1144(02)00003-1

Valentine, R.J. (2013). "An assessment of the factors that contribute to the poor performance of geosynthetic-reinforced earth retaining walls." *Proceedings of Design and Practice of Geosynthetic-Reinforced Soil Structures,* Bologna, Italy.

Watanabe, K., Nakajima, S., Fujii, K., Matsuura, K., Kudo, A., Nonaka, T., and Aoyagi, Y. (2020). "Development of geosynthetic-reinforced soil embankment resistance to severe earthquakes and prolonged overflows due to tsunamis." *Soils and Foundations*, **60**(6), 1371-1386.
https://doi.org/10.1016/j.sandf.2020.08.006

Wu, J.T.H. (2019). *Geosynthetic Reinforced Soil (GRS) Walls*, John Wiley and Sons, Ltd.

Yang, K.H., Thuo, J.N., Chen, J.W., and Liu, C.N. (2019a). "Failure investigation of a geosynthetic-reinforced soil slope subjected to rainfall." *Geosynthetics International*, **26**(1), 42-65.
https://doi.org/10.1680/jgein.18.00035

Yang, K.-H., Nguyen, T.S., Lee, Y.-H., and Leshchinsky, B. (2019b). "Performance and design of geosynthetic-reinforced soil slopes against rainfall: Considering regional hydrological conditions." *Geosynthetics International,* **26**(5), 451-473.
https://doi.org/10.1680/jgein.19.00031

Yang, K.-H., Thuo, J. N., Huynh, V.D.A., Nguyen, T.S., and Portelinha, F.H.M. (2018). "Numerical evaluation of reinforced slopes with various backfill-reinforcement-drainage systems subject to rainfall infiltration." *Computers and Geotechnics,* **96**, 25-39. https://doi.org/10.1016/j.compgeo.2017.10.012

Yang, K.-H., Yalew, W.M., and Nguyen, M.D. (2016). "Behavior of geotextile-reinforced clay with a coarse material sandwich technique under unconsolidated-undrained triaxial compression." *International Journal of Geomechanics,* ASCE, **16**(3), 04015083.
https://doi.org/10.1061/(ASCE)GM.1943-5622.0000611

Yasuhara, K. and Recio-Molina, J. (2007). "Geosynthetic-wrap around revetments for shore protection." *Geotextiles and Geomembranes.*, **25**(4-5), 221-232.

Yoo, C. and Jung, H.-Y. (2006). "Case history of geosynthetic-reinforced segmental retaining wall failure." *Journal of Geotechnical and Geoenvironmental Engineering*, ASCE, **132**(12), 1538-1548.
https://doi.org/10.1061/(ASCE)1090-0241(2006)132:12(1538)

Zornberg, J.G. and Mitchell, J.K. (1994). "Reinforced soil structures with poorly draining backfills." Part I: reinforcement interactions and functions. *Geosynthetics International*, **1**(2), 103-148. https://doi.org/10.1680/gein.1.0006